ADVANCED ENERGY MATERIALS
www.advenergymat.de

A Low-Cost Quasi-Solid-State "Water-in-Swelling-Clay" Electrolyte Enabling Ultrastable Aqueous Zinc-Ion Batteries

Siyu Tian, Taesoon Hwang, Sina Malakpour Estalaki, Yafen Tian, Long Zhou, Tye Milazzo, Seunghyun Moon, Shiwen Wu, Ruda Jian, Kenneth Balkus Jr, Tengfei Luo, Kyeongjae Cho,* and Guoping Xiong**

The poor reversibility of Zn metal anodes arising from water-induced parasitic reactions poses a significant challenge to the practical applications of aqueous zinc-ion batteries (AZIBs). Herein, a novel quasi-solid-state "water-in-swelling-clay" electrolyte (WiSCE) containing zinc sulfate and swelling clay, bentonite (BT), is designed to enable highly reversible Zn metal anodes. AZIB full cells based on the WiSCE exhibit excellent cyclic stability at various current densities, long shelf life, low self-discharge rate, and outstanding high-temperature adaptability. Particularly, the capacity of WiSCE-based AZIB full cells retains 90.47% after 200 cycles at 0.1 A g^{-1}, 96.64% after 2000 cycles at 1 A g^{-1}, and 88.29% after 5000 cycles at 3 A g^{-1}. Detailed density functional theory calculations show that strong hydrogen bonds are formed between BT and water molecules in the WiSCE. Thus, water molecules are strongly confined by BT, particularly within the interlayers, which significantly inhibits water-induced parasitic reactions and greatly improves cyclic stability. Compared to the state-of-the-art "water-in-salt" electrolytes, the WiSCE can provide a significantly higher capacity at the full-cell level with a substantially reduced cost, which is promising for the design of next-generation high-performance AZIBs. This work provides a new direction for developing cost-competitive AZIBs as alternatives to grid-scale energy storage.

1. Introduction

Aqueous zinc-ion batteries (AZIBs) have attracted tremendous research interest for grid-scale energy storage applications because of their advantages, such as low safety risks, abundant elemental resources, low cost, and eco-friendliness.[1,2] Although the electrochemical performance of AZIBs has been improved over the past few years, significant challenges impeding their practical use remain due to the ubiquitous water-induced issues at the Zn/electrolyte interface such as water decompositions (e.g., hydrogen evolution reaction – HER), zinc corrosion, byproduct passivation, and dendrite growth.[3,4] These issues can cause fast performance degradation, rapid self-discharge, and quick catastrophic failure of AZIBs. Furthermore, Zn metal anodes continuously react with water over long-term resting, leading to the unsatisfactory shelf life of AZIBs.[5] At elevated temperatures, water-induced parasitic reactions become more severe owing to accelerated chemical reactions,[5,6] which further hinders the widespread applications of AZIBs.

To date, many strategies have been proposed to address water-induced challenges, including Zn surface modification,[7,8] Zn crystallography modulation,[9,10] separator functionalization,[11,12] and electrolyte engineering.[13,14] Compared with other strategies, electrolyte engineering has emerged as a promising approach to advance the large-scale implementation of AZIBs. By tailoring the electrolyte compositions with low-cost additives, the electrochemical performance, safety, and cost-competitiveness of AZIBs are likely to be enhanced simultaneously.[15] As summarized in Table S1 (Supporting Information), a wide range of additives have been added to baseline electrolytes (e.g., 1–3 M $ZnSO_4$ in water), including inorganic oxides,[16–18] soluble salts,[19–21] polymers,[22–24] graphene quantum dots,[25] and small organic molecules.[26–28] However, grid-scale energy storage devices mainly operate at current rates (C-rates, 1 C means that a battery can be fully charged or discharged in an hour) lower than 0.5 C with peak rates up to 10 C (i.e., 6 min per charge or discharge).[29] Unfortunately,

S. Tian, L. Zhou, S. Wu, R. Jian, G. Xiong
Department of Mechanical Engineering
The University of Texas at Dallas
800 W Campbell Rd, Richardson, TX 75080, USA
E-mail: guoping.xiong@utdallas.edu
T. Hwang, K. Cho
Department of Material Science Engineering
The University of Texas at Dallas
800 W Campbell Rd, Richardson, TX 75080, USA
E-mail: kjcho@utdallas.edu
S. Malakpour Estalaki, T. Milazzo, S. Moon, T. Luo
Aerospace and Mechanical Engineering
University of Notre Dame
Notre Dame, IN 46556, USA
E-mail: tluo@nd.edu
Y. Tian, K. Balkus Jr
Department of Chemistry & Biochemistry
The University of Texas at Dallas
800 W Campbell Rd, Richardson, TX 75080, USA
The ORCID identification number(s) for the author(s) of this article can be found under https://doi.org/10.1002/aenm.202300782

DOI: 10.1002/aenm.202300782

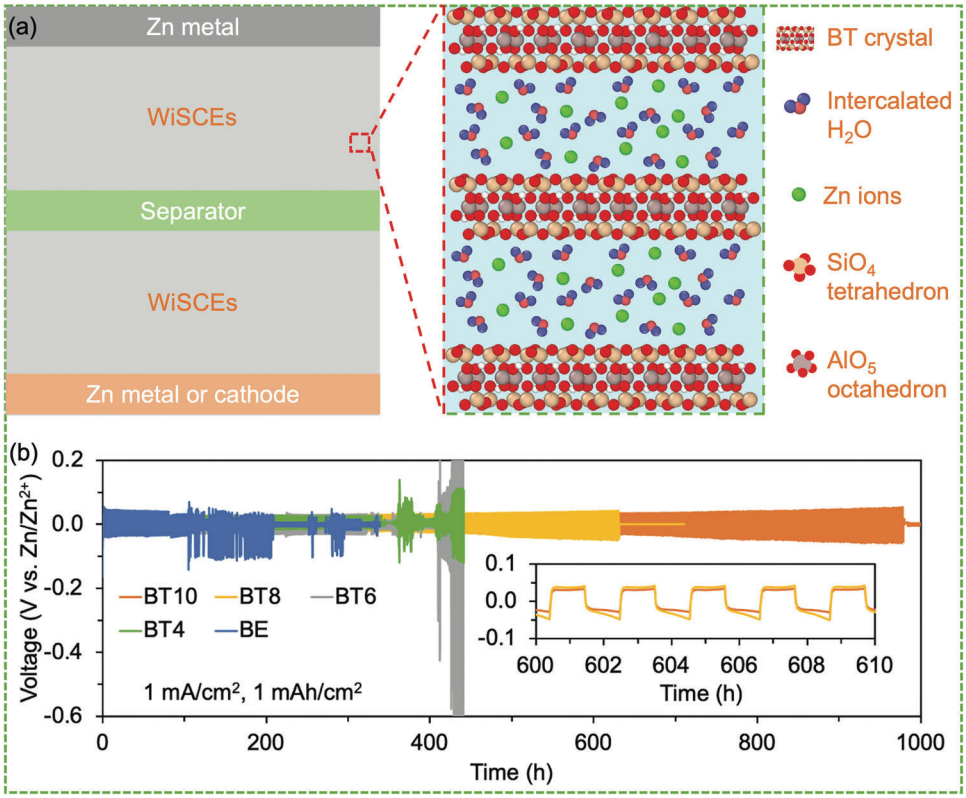

Figure 1. a) Schematic illustration of the configuration of WiSCE-based cells. b) Cyclic stability of Zn||Zn symmetric cells based on BE and WiSCEs with different BT contents at a current density of 1 mA cm^{-2} and an areal capacity of 1 mAh cm^{-2}, inset shows the voltage profiles of BT8- and BT10-based Zn||Zn symmetric cells after cycling for 600 h.

the majority of electrolyte additives (Table S1, Supporting Information) have limited effect in enhancing the cyclic stability of AZIBs at low C-rates (≤1 C) or low current densities (≤1 A g^{-1}). This is because a high cycle number but a short run time of AZIBs achieved at high C-rates can tremendously underrate the irreversibility of time-dependent, water-induced parasitic reactions, such as HER and Zn corrosion, which has been elaborated in several reviews.[30–32] Moreover, the high cost and limited material availability of conventional additives adversely affect the advantages of AZIBs as economic and scalable alternatives in grid-scale stationary energy storage applications. Therefore, finding low-cost and high-availability electrolyte additives that can simultaneously improve the long-term stability of AZIBs remains a daunting task for their practical applications in grid-scale energy storage.

Herein, a low-cost, quasi-solid-state "water-in-swelling-clay" electrolyte (WiSCE) was designed to provide a favorable aqueous environment for highly reversible Zn metal anodes. The WiSCE was prepared by mixing a high concentration (50% weight/volume, w/v) of swelling clay, bentonite (BT, $Al_2H_2O_{12}Si_4$), with the baseline electrolyte (BE, 2 M $ZnSO_4$ in water). The resulting WiSCE possessed a low salt concentration (1.2 M), high ionic conductivity (16.8 mS cm^{-1}), and an increased storage modulus (1.1 MPa). Furthermore, water molecules could be effectively confined within the interlayers of BT crystals, leading to significantly suppressed water activities toward Zn metal anodes and thus highly reversible Zn plating/stripping in the WiSCE. In addition, the WiSCE-based AZIB full cells exhibited high Coulombic efficiency (>99.9%), long shelf life (>60 days), ultralow self-discharge rate (1.89 mV per day), outstanding high-temperature adaptability (50°C), and excellent cyclic stability at low and high C-rates. This work provides a new design of a cost-competitive aqueous electrolyte to design safe, durable, and reliable AZIBs. Moreover, this work opens up a new path for designing high-performance aqueous electrolytes based on swelling clays.

2. Results and Discussion

2.1. Electrolyte Design Principles

Figure 1a schematically illustrates the configuration of WiSCE-based symmetric and full cells, in which an equal amount of WiSCE was uniformly pasted on each surface of the two electrodes (e.g., Zn metal anode or cathode). BT, or the synonym of montmorillonite, has two silica tetrahedral sheets (SiO_4) and a sandwiched alumina octahedral (AlO_5) sheet with extraordinary hydration swelling capability.[33] Once immersed into aqueous electrolytes, a significant amount of water molecules could be intercalated into BT crystals, a phenomenon known as interlayer swelling.[34–36] We hypothesize that water activities can be remarkably suppressed by confining water molecules within the interlayers of such mineral clays with excellent swelling capabilities, preventing Zn metal anodes from water-induced parasitic

reactions, and thus enhancing their reversibility in aqueous environments.

As a proof-of-concept, Zn||Zn symmetric cells based on the WiSCEs with different BT contents were assembled and cycled at 1 mA cm^{-2} and 1 mAh cm^{-2} (Figure 1b). The WiSCEs were denoted as BT*x*, where *x* represents the mass of BT per 10 mL of BE. For instance, the WiSCEs with 4 and 10 g of BT in 10 mL of BE were denoted as BT4 and BT10, respectively. The results showed that the cycle life of Zn||Zn symmetric cells increased with increasing BT content since more water molecules could be effectively confined by BT. Notably, the BT10-based symmetric cell displayed the longest cycle life of 980 h. In sharp contrast, the BE-based symmetric cell sustained less than 80 h with a sudden drop in voltage hysteresis. Meanwhile, after cycling for 600 h, the overpotential of the BT10-based Zn||Zn symmetric cell was lower than that of the BT8-based symmetric cell, suggesting that the Zn metal anode exhibited better reversibility in the BT10 electrolyte. Similarly, as shown in Figure S1 (Supporting Information), the WiSCE-based AZIB full cells exhibited better cyclic stability when increasing the BT concentrations, and the BT10-based battery displayed the best electrochemical performance during long-term cycling. With the further increase in BT concentration, the BT12-based Zn||NVO full cell exhibited excellent cyclic stability but lower capacities due to insufficient electrode-electrolyte wetting (Figure S1, Supporting Information). Therefore, BT10 is considered the optimal electrolyte for assembling Zn||NVO full cells. Most importantly, other natural clays or inorganic materials with similar chemical compositions but without interlayer swelling capabilities, such as kaolinite (KL, $Al_2H_4O_9Si_2$) and silicon dioxide (SiO_2) could not enhance the cyclic stability of full cells when added to BE as comparisons (Figures S2 and S3, Supporting Information). For KL or SiO_2, water molecules can only be absorbed on the particle surfaces, resulting in limited confinement effects and thus poor cyclic stability of AZIB full cells. Such a comparison between BT and KL (or SiO_2) highlighted the significance of confining water molecules within the interlayers. Moreover, BT has been widely used in industry with a low cost (≈$90 per ton with freight cost) and high yield (≈21 million metric tons in 2020),[37,38] rendering it the most cost-competitive electrolyte additive for AZIBs to the best of our knowledge, as summarized in Table S1 (Supporting Information). For instance, the state-of-the-art "water-in-salt" electrolyte,[39] 1 mol $Zn(TFSI)_2$ and 20 mol LiTFSI in 1 kg of water, costs $6.87 million per metric ton, which is 7438 times higher than the cost ($924 per metric ton) of the WiSCE (see detailed cost estimation in Supporting Information). Importantly, the WiSCE-based full cell exhibited a significantly higher capacity (313 mAh g^{-1} at 0.4 C) than that (100 mAh g^{-1} at 0.2 C) of the previously reported AZIB full cell based on the "water-in-salt" electrolyte.[39]

2.2. Electrolyte Properties and Structures

The BT powder exhibited an irregular flake-like shape with an average particle size of less than 10 µm (Figure S4, Supporting Information) and consisted of Si, Al, and O, as confirmed by X-ray photoelectron spectroscopy (Figure S5, Supporting Information). Upon adding high concentrations of BT into the BE, the resulting WiSCEs turned into a quasi-solid-state (Figure S6, Supporting Information) due to the formation of gel structures between BT plates.[40] **Figure 2**a shows the exact water contents in the WiSCEs determined by thermogravimetric analysis (TGA) tests. The BT powder contained 8% of physically adsorbed water, which rapidly evaporated before the temperature reached 100°C. In the WiSCEs, water content monotonically decreased with increasing BT concentration. Remarkably, the water content in BT10 decreased to 39.0 wt.% (Figure S7, Supporting Information), much lower than those of the BE (75.3 wt.%) and other WiSCEs (e.g., BT4–BT8) with lower BT concentrations. Moreover, the complete loss of water in the WiSCEs was significantly delayed up to 170 °C, suggesting that water molecules were strongly bounded to the BT host.

The existence of interlayer water in the WiSCEs was evidenced by X-ray diffraction (XRD) tests, as shown in Figure 2b. The BT powder showed an initial basal spacing (d_{001}) of 12.2 Å and several characteristic diffraction peaks of montmorillonite at 7°, 20°, 29°, 35°, and quartz at 27°.[41] The BT crystals in all the WiSCEs possessed the same d_{001} of 18.9 Å after water intercalation, corresponding to an enlarged interlayer spacing from 2.6 to 9.3 Å (Figure S8, Supporting Information).[42] This is in good agreement with the phenomenon observed in prior work, in which the swelling of BT crystals reached equilibrium with a d_{001} of ≈19.0 Å when the water content exceeded the threshold of 28.6 wt.%.[43] Note that the swelling of BT crystals induced by water intercalation exerted negligible impact on the volume of WiSCEs since the volume of the BT-BE mixture remained constant. Concurrently, the density of the BT10 electrolyte increased to ≈1.56 g cm^{-3}, slightly higher than that (1.31 g cm^{-3}) of the BE. Therefore, a slight decrease in the gravimetric energy density of the BT10-based Zn||NVO full cells can be expected in comparison to BE-based batteries. Based on the interlayer spacing, a volume expansion ratio (ER) of 54.9% of the swelled BT in the BT10 electrolyte could be determined according to the method described in prior work,[44] which suggested that ≈35.6 vol.% of free water from the BE was confined within the interlayers of BT crystals (see calculation details in Supporting Information). Additionally, water molecules could also be adsorbed on the external surface of BT,[45–47] resulting in significantly decreased amounts of free water and low water activities in the WiSCEs. Moreover, the enlarged interlayer spacing not only accommodated more water molecules between BT layers but also facilitated ion transport through the nanochannels in the viscous quasi-solid-state electrolytes. Consequently, BT10 still maintained a high ionic conductivity of 16.8 mS cm^{-1} (Figure 2c) given the ultrahigh viscosity (1363.4 Pa · s) and diluted salt concentration (1.2 M, Figure S9, Supporting Information) upon BT addition. In comparison, BE with a salt concentration of 2 M exhibited an ionic conductivity of 51.9 mS cm^{-1} and a low viscosity of 6.6 Pa · s. Furthermore, the BT10 electrolyte exhibited a transference number of 0.6 (Figure S10, Supporting Information), higher than those (ranging from 0.2 to 0.4) of the BEs reported in previous studies.[48,49] In the WiSCEs, the unique layered structure of BT may enable the formation of fast ion-conducting pathways, which can reduce ion diffusion length and facilitate fast ion transport.[50] The addition of BT also affected the pH of the WiSCEs because of the hydrolysis of BT and the adsorption of Zn ions.[51,52] For the electrolytes ranging from BT4 to BT10, their pH values stabilized at ≈5.5 (Figure S11, Supporting Information), which could alleviate Zn corrosion

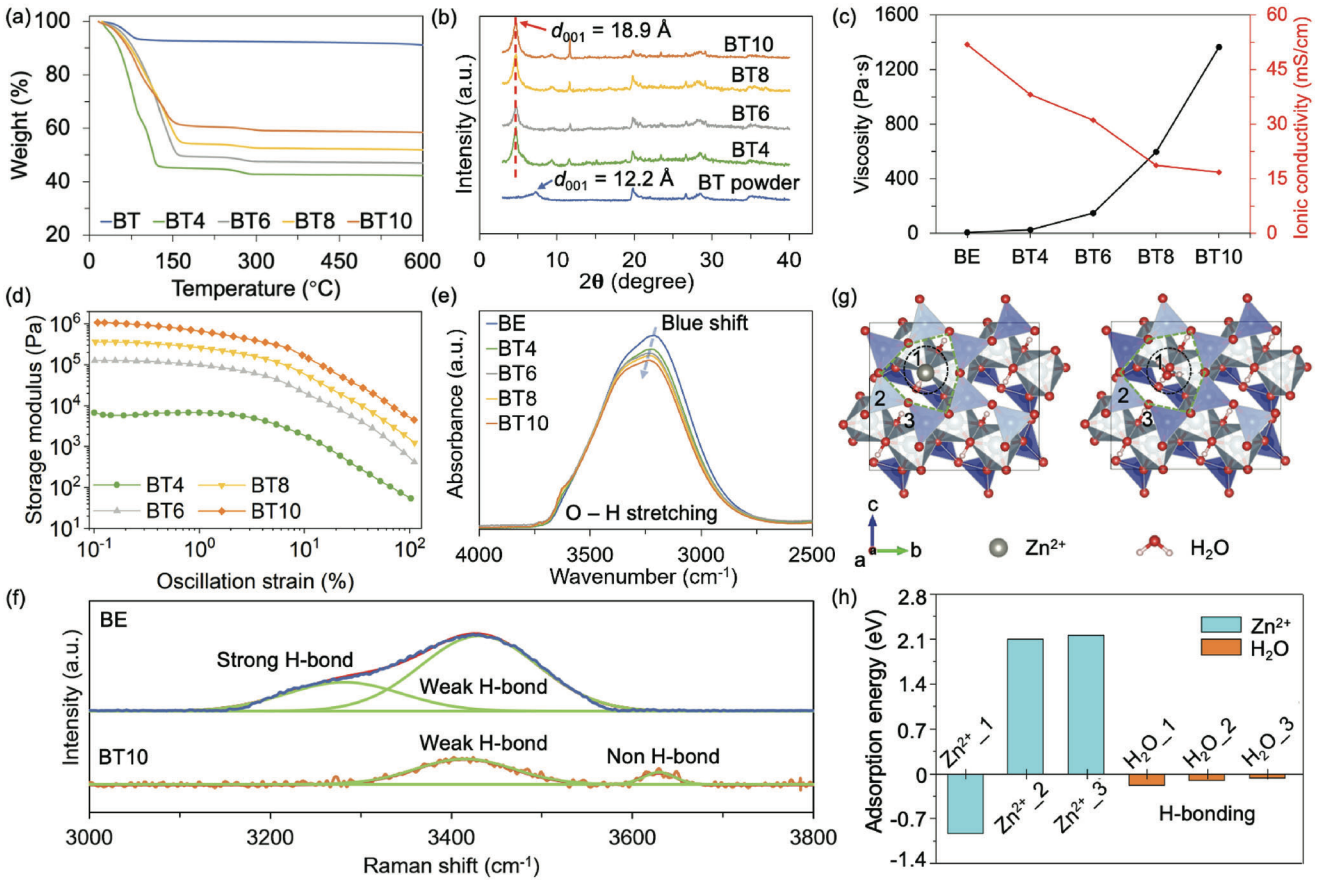

Figure 2. Physical and chemical properties of BE and WiSCEs. a) TGA curves. b) XRD curves. c) Ionic conductivities and viscosities. d) Storage modulus. e) FTIR spectra. f) Raman spectra. g) Atomic surface model of Zn^{2+} and H_2O adsorption at site 1 (Zn^{2+}_1 and H_2O_1) of the BT crystal. h) Adsorption energies of Zn^{2+} and H_2O at different sites.

and hydrogen evolution in such near-neutral environments.[20] In terms of viscoelastic properties, BT10 electrolyte exhibited the highest storage modulus (G') of 1.07 MPa (Figure 2d), signifying its superior mechanical resistance against Zn dendrite growth.[53,54] Moreover, the WiSCEs exhibited solid-like rheological properties (Figure S12, Supporting Information) due to the formation of gel structures,[33,55] which is highly desired in practical applications vulnerable to electrolyte leakage.[56,57]

To further unveil the interactions between water molecules and BT, Fourier-transform infrared (FTIR) spectroscopy, Raman spectroscopy, and nuclear magnetic resonance (NMR) spectroscopy were conducted. In the FTIR spectra (Figure 2e; Figure S13, Supporting Information), the broad peak ranging from 2700 to 3700 cm^{-1} because of O–H stretching vibration shifted to higher wavenumbers with a steadily decreased magnitude when increasing the concentration of BT. This implied strengthened hydrogen-bonding (H-bonding) interactions between water and BT and weakened H-bonding interactions among water molecules.[58–60] The chemical environment of water was further investigated by Raman tests, as shown in Figure 2f. Compared with BE, the O–H stretching vibration in the Raman spectrum of BT10 electrolyte was largely suppressed because of the limited amounts of free water molecules.[49] Moreover, in the Raman spectrum of BE, the broad peak of O–H stretching vibration can be convolved into two major peaks located at 3280 and 3430 cm^{-1} corresponding to water molecules with strong and weak H-bonds,[61] respectively. In the BT10 electrolyte, the H-bonds between water molecules were significantly weakened. In detail, the peak assigned to water molecules with strong H-bonds was absent, and a new peak located at 3630 cm^{-1} appeared because of non-hydrogen-bound water molecules.[61] These results suggested that the addition of BT effectively reconstructed the H-bonding networks between water molecules and resulted in low water activities in the BT10 electrolyte. The stretching vibrations of SO_4^{2-} located at 454 and 623 cm^{-1} were also largely blueshifted (Figure S14, Supporting Information) in the presence of BT, implying the potential changes in solvation environments.[62] Figure S15 (Supporting Information) shows the NMR spectra of the BT-BE mixtures with different BT concentrations. However, the ^2H NMR peaks of the BT-BE mixtures were not visible due to the presence of suspended BT particles.

To validate the experimental results, the adsorption of H_2O and Zn^{2+} onto the surface of BT crystals was examined by density functional theory (DFT) calculations, as shown in Figure 2g. Three adsorption configurations (Figures S16 and S17, Supporting Information) were defined due to the symmetry of the (001) basal plane of BT crystals. Figure 2h shows the adsorption energies of Zn^{2+} and H_2O at different sites. At site 1, the center of the

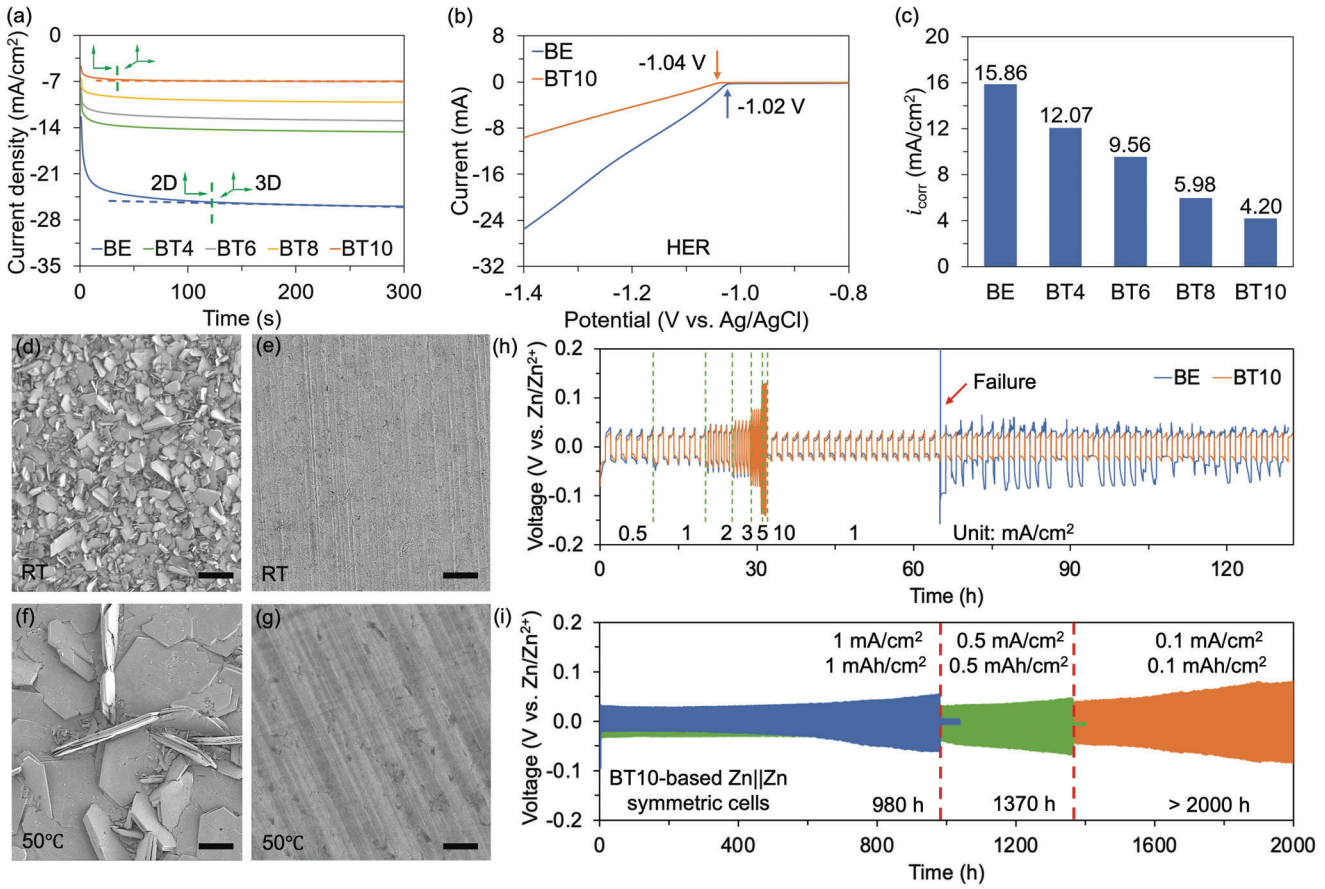

Figure 3. a) CA curves of BE and WiSCEs with different amounts of BT. b) LSV curves of BE and BT10 electrolytes. c) The corrosion current densities of Zn metal electrodes in the WiSCEs fitted from Tafel curves. SEM images of Zn metal soaked in (d) BE and (e) BT10 electrolytes for 30 days at room temperature (RT). SEM images of Zn metal soaked in (f) BE and (g) BT10 electrolytes for 10 days at 50 °C. Scale bar: d–g) 50 µm. h) Rate capability of Zn||Zn symmetric cells in BE and BT10 electrolytes. i) Cyclic stability of BT10-based Zn||Zn symmetric cells at different current densities and areal capacities.

hexagon-like oxygen rings, Zn^{2+} adsorption was thermodynamically stable, with an adsorption energy of −0.96 eV attributed to the Coulombic interactions between Zn^{2+} and oxygen atoms on the BT surface. The strong Zn^{2+} adsorption of BT could potentially alter the solvation environment of Zn^{2+} and their diffusion pathways, thus facilitating fast ion diffusions and reversible Zn plating/stripping. In comparison, Zn^{2+} adsorption was not stable at sites 2 and 3 near the Si atoms since the two sites were positively charged, as shown in Figure S18 (Supporting Information). Nevertheless, molecular dynamics simulations (Figure S19, Supporting Information) indicated that the Zn ions existing within the BT interlayers or in BE possessed the same solvation structure with a coordination number of 6 (Figure S20, Supporting Information) since the interlayer spacing (9.3 Å) of swelled BT is larger than the size (8.6 Å) of solvated zinc ions, $Zn^{2+}(H_2O)_6$.[63] Meanwhile, stable water adsorptions were observed on the entire BT surface, with the lowest adsorption energy of −0.18 eV at site 1, suggesting the excellent hydration swelling capabilities of BT. Notably, at site 1, a strong H-bond was formed between the adsorbed H_2O and the oxygen atom on the BT surface (Figure S16a, Supporting Information). These results implied that the strong water adsorption by BT was enabled by the formation of H-bonds between the two species, which further resulted in the low water activities in the quasi-solid-state WiSCEs.

2.3. Stability of the Zn Metal Anodes in the WiSCEs

Figure 3a shows the comparative chronoamperometry (CA) curves of the Zn metal electrodes in BE and WiSCEs with a constant overpotential of −150 mV. In BE, the current density of the Zn metal electrode increased rapidly over 120 s, indicating a long 2D diffusion process and a remarkable tipping effect induced by Zn dendrite growth.[64,65] On the contrary, Zn plating in the WiSCEs quickly developed into a stable 3D diffusion process after a short period (≈30 s) of Zn nucleation and 2D diffusion. This result suggested the formation of a smooth and flat Zn/electrolyte interface owing to localized Zn^{2+} reduction and uniform Zn deposition in the WiSCEs.[65] The HER behavior of Zn metal electrodes in BE and BT10 electrolytes was investigated by linear sweep voltammetry (LSV) tests, as shown in Figure 3b. In the BT10 electrolyte, the HER onset potential was delayed to −1.04 V versus Ag/AgCl with a low current during the hydrogen evolution process, which could be attributed to the limited

free water molecules, low water activities, and near-neutral pH (≈5.5) environment of the quasi-solid-state electrolyte. The oxygen evolution reaction (Figure S21, Supporting Information) was also retarded and suppressed in the BT10 electrolyte, suggesting the high stability of water molecules.

The comparative anti-corrosion performance of Zn metal in BE and WiSCEs was investigated by Tafel and soaking tests. As shown in Figure 3c, the high corrosion current density (i_{corr} = 15.86 mA cm^{-2}) indicated the aggressive corrosion of Zn metal in BE. In WiSCEs, the i_{corr} monotonically decreased to 4.20 mA cm^{-2} in BT10 when increasing the BT content. The Zn metal electrodes also exhibited more negative corrosion potentials (≈−1.01 V vs Ag/AgCl) in WiSCEs compared with that (−1.00 V vs Ag/AgCl) in BE (Figure S22, Supporting Information). These results reflected the low corrosion rate and excellent corrosion resistance of Zn metal in the WiSCEs due to the effective suppression of water activities. The extraordinary anti-corrosion performance of Zn metal in the highly concentrated WiSCEs was further confirmed by soaking tests. After being soaked in BE for 30 days at room temperature, the pristine smooth Zn surface (Figure S23, Supporting Information) was passivated by numerous flake-like byproducts (Figure 3d), indicating the severe corrosion and passivation of Zn in the mildly acidic electrolyte. In contrast, the Zn metal soaked in BT10 electrolyte under the same conditions remained nearly intact and free of precipitated byproducts (Figure 3e; Figure S24a, Supporting Information). At an elevated temperature of 50 °C, the Zn metal after being soaked in BE for 10 days was intensely passivated with large flakes of zinc sulfate hydroxide hydrate (ZHS) byproducts, including $Zn_4SO_4(OH)_6 \cdot 0.5H_2O$, $Zn_4SO_4(OH)_6 \cdot H_2O$, $Zn_4SO_4(OH)_6 \cdot 3H_2O$, $Zn_4SO_4(OH)_6 \cdot 4H_2O$, and $Zn_4SO_4(OH)_6 \cdot 5H_2O$, as shown in Figure S25 (Supporting Information). In contrast, the Zn metal demonstrated superior corrosion resistance in the BT10 electrolyte and exhibited a flat and corrosion-free surface (Figure 3g; Figure S24b, Supporting Information) under the same conditions. As evidenced by the XRD tests shown in Figure S25 (Supporting Information), only a slight byproduct of $Zn_4SO_4(OH)_6 \cdot H_2O$ was formed on the Zn metal surface when soaked in the BT10 electrolyte. Moreover, the rate of hydrogen evolution during the soaking test was quantified using an analytical balance (see details in Supporting Information). As shown in Figure S26 (Supporting Information), the hydrogen generation rate reached 28 μmol (h · cm^2)$^{-1}$ or 0.68 mL (h · cm^2)$^{-1}$ in BE, while no hydrogen evolution was observed in the BT10 electrolyte.

Zn||Zn and Cu||Zn cells were assembled to investigate the reversibility of Zn metal anodes in the WiSCEs. As shown in Figure S27a,b (Supporting Information), abundant byproducts and porous Zn deposits were formed on the surface of Zn metal anodes during long-term cycling, which resulted in a short cycle life of the BE-based symmetric cell. However, in the BT10 electrolyte, the cycled Zn metal anode exhibited a dendrite-free morphology (Figure S27c,d, Supporting Information) because of the significantly suppressed hydrogen evolution, Zn corrosion, and dendrite growth. Therefore, the cycle life of the BT10-based Zn||Zn symmetric cell could be significantly prolonged to 980 h with lower voltage hysteresis (Figure S28, Supporting Information). Nevertheless, as confirmed by SEM (Figure S27c, Supporting Information) and XRD (Figure S29, Supporting Information) data, a small amount of $Zn_4SO_4(OH)_6 \cdot H_2O$ byproduct was formed on the surface of the Zn metal anode during long-term cycling, resulting in gradually increased voltage hysteresis of the Zn||Zn symmetric cells.[14] As shown in Figure S30 (Supporting Information), the BT10-based Zn||Zn symmetric cell also exhibited a lower charge transfer resistance of 230 Ω compared with that (270 Ω) of the BE-based Zn||Zn cell, implying its fast kinetics during Zn plating/stripping.

Figure 3h shows the rate capabilities of the Zn||Zn symmetric cells based on BE and BT10 electrolytes. The BT10-based symmetric cell exhibited a stable voltage profile with low voltage hysteresis upon changing current densities. The overpotentials of the BT10-based Zn||Zn symmetric cells monotonically increased from 26.9 mV at 0.5 mA cm^{-2} to 123.8 mV at 10 mA cm^{-2} at a constant areal capacity of 1 mAh cm^{-2} (Figure S31, Supporting Information), agreeing well with the trend observed in previous studies.[66,67] Comparatively, the BE-based symmetric cell quickly failed when switching the current density from 10 to 1 mA cm^{-2}. As shown in Figure 3i, when cycled at lower areal capacities of 0.5 and 0.1 mAh cm^{-2} with a C-rate of 1 C, the cycle life of the BT10-based symmetric cells could be further extended to 1370 and 2000 h, respectively. In contrast, the BE-based Zn||Zn symmetric cells generally failed after cycling for ≈100 h (Figure S32, Supporting Information) due to fast dendrite growth and severe water-induced parasitic reactions. The enhanced Zn plating/stripping reversibility could be mainly attributed to the low water activities and high mechanical stiffness of the quasi-solid-state BT10 electrolyte, making it effective in suppressing HER, Zn corrosion, and dendrite growth over long-term cycling. As shown in Figure S33 (Supporting Information), at a constant rate of 1 C (i.e., plating or stripping for 1 h), the BT10-based Zn||Zn symmetric cells exhibited initial nucleation overpotentials of −32, −75, and −99 mV at 0.1, 0.5, and 1 mA cm^{-2}, respectively. This suggested that more Zn nuclei were formed on the Zn metal surface at 1 mA cm^{-2} and 1 mAh cm^{-2}.[66,68] During the following plating process, the reduction of Zn^{2+} on the nucleus was much easier than on the uncycled Zn surface, leading to a significant reduction in the plating overpotential at the equilibrium stage.[69] Therefore, the equilibrium plating overpotential of the BT10-based Zn||Zn symmetric cell at 1 mA cm^{-2} and 1 mAh cm^{-2} was lower than that at 0.5 mA cm^{-2} and 0.5 mAh cm^{-2} (or 0.1 mA cm^{-2} and 0.1 mAh cm^{-2}), similar to the phenomenon observed in prior work.[9] Meanwhile, the quasi-solid-state BT10 electrolyte significantly inhibited water-induced parasitic reactions that would otherwise result in low Coulombic efficiency (CE) during Zn plating/stripping. As shown in Figure S34 (Supporting Information), the BE-based Cu||Zn half-cell possessed a low initial CE of 83.75% and failed after 60 cycles at 1 mA cm^{-2}. In comparison, the initial CE of the BT10-based Cu||Zn half-cell increased to 96.87%, and a high average CE of 99.53% was achieved during the cycling, confirming remarkably inhibited water-induced parasitic reactions in the quasi-solid-state BT10 electrolyte. Furthermore, the nucleation overpotential dropped dramatically from 41 to 12 mV (Figure S35, Supporting Information), suggesting a lower energy barrier for Zn reduction in the BT10 electrolyte, which is conducive to the uniform nucleation and deposition of Zn metal.[28] The low Zn nucleation energy barrier, fast interfacial charge transfer kinetics, and rapid Zn^{2+} migration ultimately resulted in the lower overpotential of

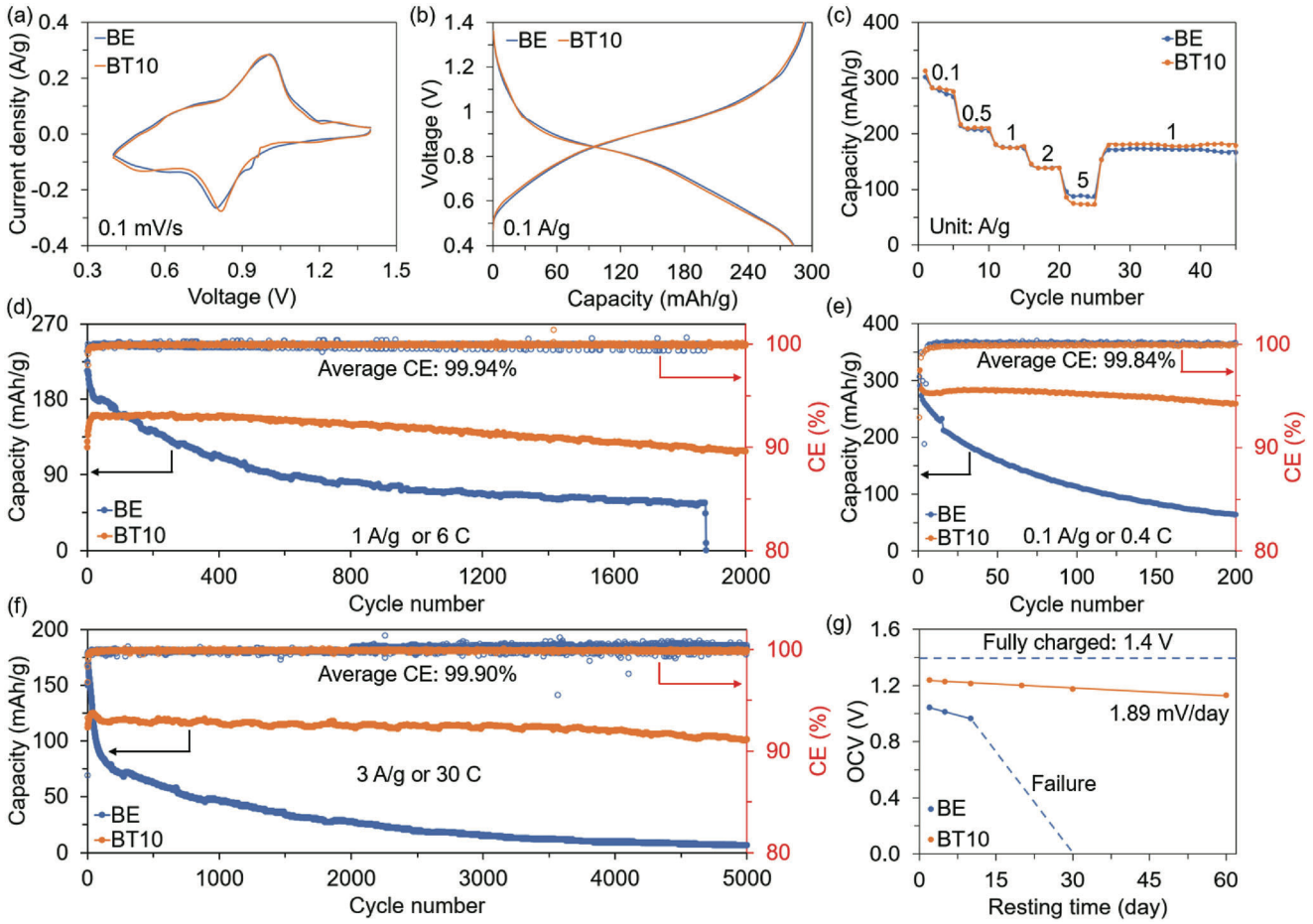

Figure 4. The electrochemical performance of Zn||NVO full cells based on BE and BT10 electrolytes. a) CV curves at a scan rate of 0.1 mV s. b) Galvanostatic charge/discharge curves at a current density of 0.1 A g. c) Rate capabilities. Long-term cyclic stability of Zn||NVO full cells based on BE and BT10 electrolytes at different current densities of d) 1, e) 0.1, and f) 3 A g^{-1}. g) Self-discharge performance of fully charged Zn||NVO full cells based on BE and BT10 electrolytes.

the BT10-based Zn||Zn symmetric cell in comparison to the BE-based device.[70]

2.4. Electrochemical Performance of the WiSCE-Based Full Cells

To demonstrate the advantages of the WiSCEs in practical applications, AZIB full cells were assembled using a widely reported cathode material, sodium-doped V_2O_5 (NVO).[71,72] **Figure 4**a,b shows the cyclic voltammetry (CV) and galvanostatic charge/discharge curves of the Zn||NVO full cells based on BE and BT10 electrolytes, respectively. Similar redox peaks during the CV test and nearly identical voltage profiles during charge/discharge were observed, suggesting that no extra redox or parasitic reactions were introduced by BT. Figure 4c shows the rate capabilities of the full cells based on the two electrolytes, in which the BT10-based cell exhibited discharge capacities of 313.0, 217.2, 181.2, 146.1, and 86.1 mAh g^{-1} at current densities of 0.1, 0.5, 1, 2, and 5 A g^{-1}, respectively. The specific capacity of the BT10-based full cell recovered to 180.1 mAh g^{-1} when the current density returned to 1 A g^{-1}, higher than that (170.8 mAh g^{-1}) of the BE-based cell. Moreover, the BT10-based full cell exhibited a lower charge transfer resistance compared with that of the BE-based cell (Figure S36, Supporting Information), consistent with the results obtained in symmetric cells.

Figure 4d–f shows the comparative long-term cyclic stability and CEs of the Zn||NVO full cells based on BE and BT10 electrolytes at three different current densities. As shown in Figure 4d, the capacity of the BT10-based full cell increased from 122.1 mAh g^{-1} at the first cycle to 160.7 mAh g^{-1} after 20 cycles at 1 A g^{-1} due to the electrochemical activation of the cathode.[73] After 1000 and 2000 cycles, the capacities of the BT10-based full cell retained 144.9 and 118.0 mAh g^{-1}, respectively. In contrast, the capacity of the BE-based full cell decayed to 71.6 mAh g^{-1} after 1000 cycles and failed after ≈1900 cycles. Note that at a constant current density of 1 A g^{-1}, the initial capacity (224.8 mAh g^{-1}, Figure 4d) of the BE-based Zn||NVO full cell during the long-term cycling tests was higher than that (181.2 mAh g^{-1}, Figure 4c) of the BE-based battery during the rate capability tests. This could be attributed to the fast capacity degradation of the BE-based battery that occurred at 0.1 and 0.5 A g^{-1} during the rate capability tests. At a lower current density of 0.1 A g^{-1}, the BT10-based full

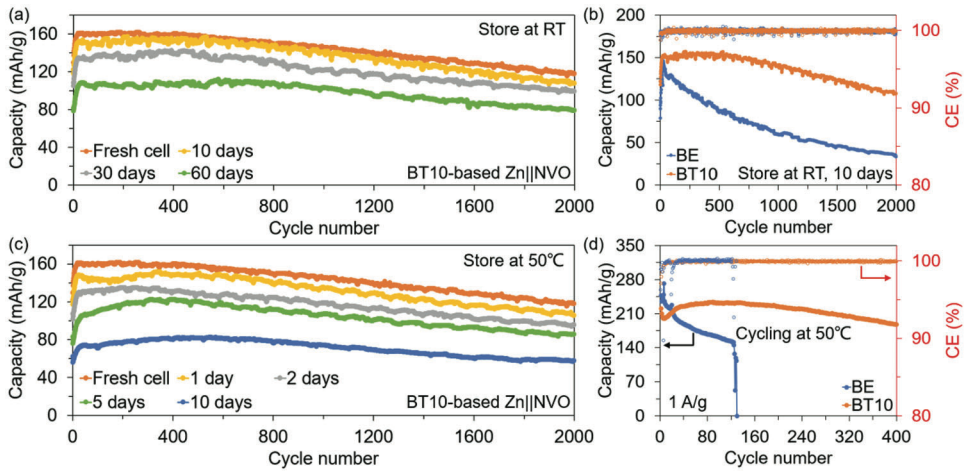

Figure 5. a) Cyclic stability of BT10-based full cells after being stored at room temperature for up to 60 days. b) Cyclic stability of BE- and BT10-based full cells after 10-day storage at room temperature. c) Cyclic stability of BT10-based full cells tested at room temperature after storage at 50°C for up to 10 days. d) Cyclic stability of fresh BT10-based full cells working at 50°C with a current density of 1 A g^{-1}.

cell displayed a high initial discharge capacity of 318.5 mAh g^{-1}, as shown in Figure 4e. The capacity decreased to 284.5 mAh g^{-1} at the 2nd cycle and retained 257.4 mAh g^{-1} at the 200th cycle, corresponding to a high retention rate of 90.47% over 200 cycles, while the BE-based full cell only retained 21.49% of its initial capacity after 200 cycles at 0.1 A g^{-1} due to the severe parasitic reactions. At a high current density of 3 A g^{-1}, the capacity of the BT10-based full cell retained 88.29% after 5000 cycles, substantially outperforming that (4.44%) of the BE-based full cell under the same condition (Figure 4f). Moreover, the CEs of the BT10-based full cells were much more stable than those of BE-based batteries at the three current densities. Note that the initial capacities of the BT10-based Zn||NVO full cells were lower than those of the BE-based Zn||NVO full cells at current densities of 1 and 3 A g^{-1}, which is likely due to the decreased electrolyte-electrode wettability resulting from the low water content, high viscosity, and high modulus of the BT10 electrolyte.[74] Compared with previously reported AZIBs with other electrolyte additives[75] and high-cost water-in-salt electrolytes,[76] the BT10-based full cells exhibited superior cyclic stability at different current densities (Table S1, Supporting Information), signifying that the WiSCE is promising for the fabrication of high-performance AZIBs. To understand the remarkably improved cyclic stability of BT10-based full cells, the morphology of the cycled Zn metal anode was characterized by SEM (Figure S37, Supporting Information). After 1000 cycles at 3 A g^{-1}, the Zn metal anode cycled in BT10 electrolyte maintained a dendrite-free morphology due to the high stiffness of the quasi-solid-state electrolyte and suppressed water activities, which is in sharp contrast with that of the Zn metal anode cycled in BE. These results confirmed that BT, a low-cost and high-availability electrolyte additive, provided a favorable aqueous environment for Zn metal anodes. Thus, the cyclability of BT10-based full cells could be significantly enhanced at low and high charge/discharge C-rates, which is highly desired in practical grid-scale energy storage applications.

In addition, Figure 4g exhibits the comparative self-discharge performance of the Zn||NVO full cells based on BE and BT10 electrolytes, which is evaluated by monitoring the open circuit voltage (OCV) of fully charged cells during rest time up to 60 days before being fully discharged to 0.4 V. Figure S38 (Supporting Information) shows the corresponding voltage profiles of the Zn||NVO full cells during resting. Because of the severe parasitic reactions, the OCV of the BE-based full cells quickly dropped to 1.04 V after resting for 2 days and retained only 0.96 V after resting for 10 days. When further extending the resting time, drastic voltage drops were observed for the BE-based full cells, indicating the failure of these batteries because of severe hydrogen evolution and Zn corrosion during long-term resting. On the contrary, for the BT10-based full cells, the OCV dropped to 1.24 V after resting for 2 days and retained 1.13 V after resting for 60 days, corresponding to an ultralow voltage decay rate of 1.89 mV per day or 0.079 mV h^{-1}, which is one order of magnitude lower than those of previously reported aqueous batteries.[77,78] Moreover, the BT10-based full cell still retained 43.74% of its charge capacity after resting for 60 days (Figure S39, Supporting Information), demonstrating that the quasi-solid-state electrolyte is highly promising for practical AZIBs that require long-term storage capabilities.

The superior long-term storage capability of the BT10-based full cells was further demonstrated by storing the assembled full cells at room temperature for up to 60 days before cyclic galvanostatic charge/discharge tests. As shown in **Figure 5**a, after 60 days of storage, the BT10-based full cell still featured extraordinary cyclic stability and a high average CE (99.94%, Figure S40, Supporting Information) over 2000 cycles at 1 A g^{-1}, indicating its ultralong shelf life and outstanding resistance to performance degradation during long-term storage. In comparison, Figure 5b exhibits that the BE-based full cell suffered from severe capacity degradation after 10-day storage and failed when further extending the storage time (Figure S41, Supporting Information). At a higher temperature of 50°C, the shelf life of the BE-based full cell was further decreased to less than 1 day (Figure S42, Supporting Information) due to the significantly accelerated hydrogen evolution and Zn corrosion. However, as shown in Figure 5c, the BT10-based full cell still exhibited excellent cyclic stability over 2000 cycles at 1 A g^{-1} after 10-day storage at 50°C, signifying its long

shelf life at elevated temperatures. Moreover, Figure 5d shows that the as-assembled BT10-based full cell could safely operate at 50°C over 400 cycles at 1 A g^{-1} and retained 84.54% of its initial capacity of 220.5 mAh g^{-1}, outperforming the high-temperature adaptability of most AZIBs reported in prior work (Table S2, Supporting Information). These results manifested the extraordinary shelf life and high-temperature adaptability of the BT10-based full cells toward practical energy storage applications.

3. Conclusion

A new type of quasi-solid-state WiSCE was developed to reduce free water contents and suppress water activities for highly reversible Zn plating/stripping in aqueous environments. By introducing a low-cost and high-availability swelling clay, BT, into the mild acidic electrolyte, water molecules could be strongly confined within the interlayers of BT crystals, leading to low water activities in the quasi-solid-state electrolyte. The formation of gel structures between BT plates also enabled the high stiffness and high viscosity of the BT-based electrolyte. Therefore, dendrite growth, Zn corrosion, and gas evolutions at the Zn/electrolyte interface could be effectively inhibited. In addition, the WiSCE-based Zn||NVO full cells exhibited excellent cyclic stability at different current densities. Particularly, the capacities of the full cells retained 90.47% after 200 cycles at 0.1 A g^{-1}, 96.64% after 2000 cycles at 1 A g^{-1}, and 88.29% after 5000 cycles at 3 A g^{-1}. This work revealed that a natural swelling clay, BT, with layered structures could effectively enhance the cyclic stability, safety, and reliability of AZIBs. Benefiting from the low cost, high availability, and facile functionalization of BT, the quasi-solid-state WiSCE with low water activities would be promising to design high-performance AZIBs and accelerate their commercialization in grid-scale energy storage applications.

Supporting Information

Supporting Information is available from the Wiley Online Library or from the author.

Acknowledgements

G.X. thanks the University of Texas at Dallas startup fund and the support from the NSF (Grant No. CBET-1937949 and CBET-1949962). T.L. thanks the support from the NSF (Grant No. CBET-1937923 and CBET-1949910) for support. K.C. thanks the support from National R&D Program (2022M3H4A1A04096496) through the National Research Foundation of Korea (NRF) funded by Ministry of Science and ICT.

Conflict of Interest

The authors declare no conflict of interest.

Data Availability Statement

The data that support the findings of this study are available from the corresponding author upon reasonable request.

Keywords

aqueous zinc-ion batteries, bentonite swelling clay, electrolytes, quasi-solid-state, Zn metal anodes

Received: March 13, 2023
Revised: June 8, 2023
Published online:

[1] D. Chao, W. Zhou, F. Xie, C. Ye, H. Li, M. Jaroniec, S. Qiao, *Sci. Adv.* **2020**, *6*, eaba4098.
[2] N. Guo, W. Huo, X. Dong, Z. Sun, Y. Lu, X. Wu, L. Dai, L. Wang, H. Lin, H. Liu, H. Liang, Z. He, Q. Zhang, *Small Methods* **2022**, *6*, 2200597.
[3] W. Du, E. Ang, Y. Yang, Y. Zhang, M. Ye, C. Li, *Energy Environ. Sci.* **2020**, *13*, 3330.
[4] W. Guo, Z. Cong, Z. Guo, C. Chang, X. Liang, Y. Liu, W. Hu, X. Pu, *Energy Storage Mater.* **2020**, *30*, 104.
[5] Z. Chen, X. Li, D. Wang, Q. Yang, L. Ma, Z. Huang, G. Liang, A. Chen, Y. Guo, B. Dong, X. Huang, C. Yang, C. Zhi, *Energy Environ. Sci.* **2021**, *14*, 3492.
[6] C. Xie, Y. Li, Q. Wang, D. Sun, Y. Tang, H. Wang, *Carbon Energy* **2020**, *2*, 540.
[7] L. Hong, L. Wang, Y. Wang, X. Wu, W. Huang, Y. Zhou, K. Wang, J. Chen, *Adv. Sci.* **2022**, *9*, 2104866.
[8] S. Tian, L. Zhou, W. He, Y. Tian, Y. Zhou, S. Wu, R. Jian, K. Balkus, T. Luo, G. Xiong, *Chem. Eng. J.* **2023**, *462*, 142276.
[9] Z. Chen, J. Zhao, Q. He, M. Li, S. Feng, Y. Wang, D. Yuan, J. Chen, H. Alshareef, Y. Ma, *ACS Energy Lett.* **2022**, *7*, 3564.
[10] S. Pu, C. Gong, Y. Tang, Z. Ning, J. Liu, S. Zhang, Y. Yuan, D. Melvin, S. Yang, L. Pi, J. Marie, B. Hu, M. Jenkins, Z. Li, B. Liu, S. Tsang, T. Marrow, R. Reed, X. Gao, P. Bruce, A. Robertson, *Adv. Mater.* **2022**, *34*, 2202552.
[11] Y. Guo, W. Cai, Y. Lin, Y. Zhang, S. Luo, K. Huang, H. Wu, Y. Zhang, *Energy Storage Mater.* **2022**, *50*, 580.
[12] J. Cao, D. Zhang, C. Gu, X. Wang, S. Wang, X. Zhang, J. Qin, Z. Wu, *Adv. Energy Mater.* **2021**, *11*, 2101299.
[13] R. Meng, H. Li, Z. Lu, C. Zhang, Z. Wang, Y. Liu, W. Wang, G. Ling, F. Kang, Q. Yang, *Adv. Mater.* **2022**, *34*, 2200677.
[14] Y. Lv, M. Zhao, Y. Du, Y. Kang, Y. Xiao, S. Chen, *Energy Environ. Sci.* **2022**, *15*, 4748.
[15] Y. Meng, V. Srinivasan, K. Xu, *Science* **2022**, *378*, eabq3750.
[16] J. Zhou, L. Zhang, M. Peng, X. Zhou, Y. Cao, J. Liu, X. Shen, C. Yan, T. Qian, *Adv. Mater.* **2022**, *34*, 2200131.
[17] J. Gao, X. Xie, S. Liang, B. Lu, J. Zhou, *Nano-Micro Lett.* **2021**, *13*, 69.
[18] J. Cao, D. Zhang, Y. Yue, R. Chanajaree, S. Wang, J. Han, X. Zhang, J. Qin, Y. Huang, *Nano Energy* **2022**, *93*, 106839.
[19] W. Zhang, Y. Dai, R. Chen, Z. Xu, J. Li, W. Zong, H. Li, Z. Li, Z. Zhang, J. Zhu, F. Guo, X. Gao, Z. Du, J. Chen, T. Wang, G. He, I. Parkin, *Angew. Chem., Int. Ed.* **2023**, *62*, e202212695.
[20] D. Han, Z. Wang, H. Lu, H. Li, C. Cui, Z. Zhang, R. Sun, C. Geng, Q. Liang, X. Guo, Y. Mo, X. Zhi, F. Kang, Z. Weng, Q. Yang, *Adv. Energy Mater.* **2022**, *12*, 2102982.
[21] Q. Zhang, Y. Ma, Y. Lu, Y. Ni, L. Lin, Z. Hao, Z. Yan, Q. Zhao, J. Chen, *J. Am. Chem. Soc.* **2022**, *144*, 18435.
[22] J. Zhou, M. Peng, X. Xia, S. Qian, Z. Wang, C. Zhu, X. Zeng, H. Ji, S. Wang, X. Zhou, J. Liu, X. Shen, Y. Cheng, T. Qian, C. Yan, *Nano Lett.* **2022**, *22*, 2898.
[23] S. Gao, J. Han, Z. Liu, K. Wang, K. Jiang, C. Guo, Y. Tan, D. Zhou, W. Shi, *J. Electrochem. Soc.* **2021**, *168*, 080514.
[24] N. Wang, Y. Yang, X. Qiu, X. Dong, Y. Wang, Y. Xia, *ChemSusChem* **2020**, *13*, 5556.

[25] H. Zhang, R. Guo, S. Li, C. Liu, H. Li, G. Zou, J. Hu, H. Hou, X. Ji, *Nano Energy* **2022**, *92*, 106752.
[26] W. Xu, K. Zhao, W. Huo, Y. Wang, G. Yao, X. Gu, H. Cheng, L. Mai, C. Hu, X. Wang, *Nano Energy* **2019**, *62*, 275.
[27] H. Zhang, Y. Zhong, J. Li, Y. Liao, J. Zeng, Y. Shen, L. Yuan, Z. Li, Y. Huang, *Adv. Energy Mater.* **2022**, *13*, 2203254.
[28] Y. Zhong, Z. Cheng, H. Zhang, J. Li, D. Liu, Y. Liao, J. Meng, Y. Shen, Y. Huang, *Nano Energy* **2022**, *98*, 107220.
[29] H. Hesse, M. Schimpe, D. Kucevic, A. Jossen, *Energies* **2017**, *10*, 2107.
[30] L. Blanc, D. Kundu, L. Nazar, *Joule* **2020**, *4*, 771.
[31] G. Zampardi, F. Mantia, *Nat. Commun.* **2022**, *13*, 687.
[32] C. Li, S. Jin, L. Archer, L. Nazar, *Joule* **2022**, *6*, 1733.
[33] P. Luckham, S. Rossi, *Adv. Colloid Interface Sci.* **1999**, *82*, 43.
[34] S. Hendricks, M. Jefferson, *Am. Min.* **1938**, *23*, 863.
[35] D. Smith, *Langmuir* **1998**, *14*, 5959.
[36] S. Pradhan, K. Katti, D. Katti, *Int. J. Numer. Anal. Methods Geomech.* **2015**, *15*, 04014073.
[37] M. Garside, https://www.statista.com/statistics/1312558/bentonite-production-volume-worldwide-by-country/ (accessed: June 2022).
[38] M. Garside, https://www.statista.com/statistics/248186/average-bentonite-price/ (accessed: February 2022).
[39] F. Wang, O. Borodin, T. Gao, X. Fan, W. Sun, F. Han, A. Faraone, J. Dura, K. Xu, C. Wang, *Nat. Mater.* **2018**, *17*, 543.
[40] K. Choo, K. Bai, *Appl. Clay Sci.* **2015**, *108*, 182.
[41] B. Salah, M. Gaber, A. Kandil, *Minerals* **2019**, *9*, 626.
[42] H. Komine, *J. Geotech. Geoenviron. Eng.* **2008**, *134*, 497.
[43] H. Wang, T. Shirakawabe, H. Komine, D. Ito, T. Gotoh, Y. Ichikawa, Q. Chen, *Can. Geotech. J.* **2019**, *57*, 921.
[44] S. Suzuki, S. Prayongphan, Y. Ichikawa, B. Chae, *Appl. Clay Sci.* **2005**, *29*, 89.
[45] D. Anderson, P. Low, *Nature* **1957**, *180*, 1194.
[46] F. Kraehenbuehl, H. Stoeckli, F. Brunner, G. Kahr, M. Vonmoos, *Clay Miner.* **1987**, *22*, 1.
[47] G. Montes, J. Duplay, L. Martinez, Y. Geraud, B. Tournier, *Appl. Clay Sci.* **2003**, *23*, 309.
[48] H. Yan, S. Li, Y. Nan, S. Yang, B. Li, *Adv. Energy Mater.* **2021**, *11*, 2100186.
[49] J. Zhu, Z. Bie, X. Cai, Z. Jiao, Z. Wang, J. Tao, W. Song, H. Fan, *Adv. Mater.* **2022**, *34*, 2207209.
[50] E. Pomerantseva, Y. Gogotsi, *Nat. Energy* **2017**, *2*, 17089.
[51] S. Kaufhold, R. Dohrmann, D. Koch, G. Houben, *Clays Clay Miner.* **2008**, *56*, 338.
[52] P. Kumararaja, K. Manjaiah, S. Datta, T. Shabeer, B. Sarkar, *Cellulose* **2018**, *25*, 3985.
[53] M. Wang, A. Emre, S. Tung, A. Gerber, D. Wang, Y. Huang, V. Cecen, N. Kotov, *ACS Nano* **2019**, *13*, 1107.
[54] C. Liu, X. Xie, B. Lu, J. Zhou, S. Liang, *ACS Energy Lett.* **2021**, *6*, 1015.
[55] H. Olphen, *Clays Clay Miner.* **1955**, *4*, 204.
[56] Y. Lv, Y. Xiao, L. Ma, C. Zhi, S. Chen, *Adv. Mater.* **2022**, *34*, 2106409.
[57] K. Wu, J. Huang, J. Yi, X. Liu, Y. Liu, Y. Wang, J. Zhang, Y. Xia, *Adv. Energy Mater.* **2020**, *10*, 1903977.
[58] K. Mizuno, Y. Miyashita, Y. Shindo, H. Ogawa, *J. Phys. Chem.* **1995**, *99*, 3225.
[59] R. Chua, Y. Cai, P. Lim, S. Kumar, R. Satish, W. Manalastas, H. Ren, V. Verma, S. Meng, S. Morris, P. Kidkhunthod, J. Bai, M. Srinivasan, *ACS Appl. Mater. Interfaces* **2020**, *12*, 22862.
[60] P. Jørgensen, *Geol. Fören. Stockh. Förh.* **1968**, *90*, 213.
[61] Q. Zhang, Y. Ma, Y. Lu, L. Li, F. Wan, K. Zhang, J. Chen, *Nat. Commun.* **2020**, *11*, 4463.
[62] K. Mabrouk, T. Kauffmann, H. Aroui, M. Fontana, *J. Raman Spectrosc.* **2013**, *44*, 1603.
[63] E. Nightingale, *J. Phys. Chem.* **1959**, *63*, 1381.
[64] C. Huang, X. Zhao, S. Liu, Y. Hao, Q. Tang, A. Hu, Z. Liu, X. Chen, *Adv. Mater.* **2021**, *33*, 2100445.
[65] Z. Zhao, J. Zhao, Z. Hu, J. Li, J. Li, Y. Zhang, C. Wang, G. Cui, *Energy Environ. Sci.* **2019**, *12*, 1938.
[66] H. Liu, Y. Zhang, C. Wang, J. Glazer, Z. Shan, N. Liu, *ACS Appl. Mater. Interfaces* **2021**, *13*, 32930.
[67] Q. Cao, Y. Gao, J. Pu, X. Zhao, Y. Wang, J. Chen, C. Guan, *Nat. Commun.* **2023**, *14*, 641.
[68] A. Pei, G. Zheng, F. Shi, Y. Li, Y. Cui, *Nano Lett.* **2017**, *17*, 1132.
[69] Q. Li, A. Chen, D. Wang, Y. Zhao, X. Wang, X. Jin, B. Xiong, C. Zhi, *Nat. Commun.* **2022**, *13*, 3699.
[70] C. Yuan, L. Yin, P. Du, Y. Yu, K. Zhang, X. Ren, X. Zhan, S. Gao, *Chem. Eng. J.* **2022**, *442*, 136231.
[71] P. He, G. Zhang, X. Liao, M. Yan, X. Xu, Q. An, J. Liu, L. Mai, *Adv. Energy Mater.* **2018**, *8*, 1702463.
[72] B. Yong, D. Ma, Y. Wang, H. Mi, C. He, P. Zhang, *Adv. Energy Mater.* **2020**, *10*, 2002354.
[73] W. Wang, V. Kale, Z. Cao, Y. Lei, S. Kandambeth, G. Zou, Y. Zhu, E. Abouhamad, O. Shekhah, L. Cavallo, M. Eddaoudi, H. Alshareef, *Adv. Mater.* **2021**, *33*, 2103617.
[74] A. Zhou, J. Zhang, M. Chen, J. Yue, T. Lv, B. Liu, X. Zhu, K. Qin, G. Feng, L. Suo, *Adv. Mater.* **2022**, *34*, 2207040.
[75] J. Zhou, M. Peng, X. Xia, S. Qian, Z. Wang, C. Zhu, X. Zeng, H. Ji, S. Wang, X. Zhou, *Nano Lett.* **2022**, *22*, 2898.
[76] Y. Zhu, J. Yin, X. Zheng, A. Emwas, Y. Lei, O. Mohammed, Y. Cui, H. Alshareef, *Energy Environ. Sci.* **2021**, *14*, 4463.
[77] R. Trócoli, A. Morata, C. Erinmwingbovo, F. Mantia, A. Tarancón, *Electrochim. Acta* **2021**, *373*, 137847.
[78] L. Suo, F. Han, X. Fan, H. Liu, K. Xu, C. Wang, *J. Mater. Chem. A* **2016**, *4*, 6639.